J|A|C|S ARTICLES

Published on Web 02/01/2010

Electrochemical Reactivity of Aromatic Molecules at Nanometer-Sized Surface Domains: From Pt(*hkl*) Single Crystal Electrodes to Preferentially Oriented Platinum Nanoparticles

Margarita Rodríguez-López,[†,§,II] Jose Solla-Gullón,[‡] Enrique Herrero,[‡] Paulino Tuñón,[§] Juan M. Feliu,[‡] Antonio Aldaz,*[,‡] and Arnaldo Carrasquillo, Jr.*[,II]

Department of Chemistry, Pontifical Catholic University of Puerto Rico, Ponce, Puerto Rico, Departamento de Química Física, Instituto Universitario de Electroquímica, University of Alicante, Alicante, Spain, University of Oviedo, Oviedo, Spain, and Department of Chemistry, University of Puerto Rico, Mayagüez, Puerto Rico 00681-9019

Received October 25, 2009; E-mail: c4rr4s4@gmail.com; arnaldo.carrasquil@upr.edu; aldaz@ua.es

Abstract: This manuscript compares the electrochemically controlled adsorption of hydroquinone-derived adlayers and their reductive desorption from nanometer-sized Pt(111) domains present on the surface (i) of model stepped single-crystal electrodes and (ii) of preferentially oriented Pt nanoparticles. The results obtained using a stepped surface series, i.e., Pt(S)[(n − 1)(111)×(110)], suggest that in the presence of 2 mM $H_2Q_{(aq)}$ the electrochemically detected desorption-adsorption process takes place selectively from ordered Pt(111) domains present as terraces, while being precluded at other available surface sites, i.e., Pt(110) steps, where adsorption takes place irreversibly. This domain-selective electroanalytical detection scheme is employed later to selectively monitor desorption-adsorption of hydroquinone-derived adlayers from ordered, nanometer-scaled Pt(111) domains on the surface of preferentially oriented Pt nanoparticles, confirming the existence of well-ordered (111) domains on the surface of the Pt nanoparticles. A good correlation is noted between the electrochemical behavior at well-ordered Pt(*hkl*) surfaces and at preferentially oriented Pt nanoparticles. Key learnings and potential applications are discussed. The results demonstrate the technical feasibility of performing domain-selective decapping of nanoparticles by handle of an externally controlled parameter, i.e., the applied potential.

1. Introduction

The study of nanometer-sized metal structures and particles has become a major subject of modern interfacial science.[1−3] This well-disserved attention is rooted to the premise that nanostructured materials,[4] and even monodispersed metal nanoparticles, can exhibit properties which differ from those of bulk metal, of molecular and of atomic species. Differences in properties between bulk-metal and nanoparticles may arise from differences in electronic structure, as when a sufficiently small number of atoms is involved, implying small particle diameters, e.g. < 5 nm, or when dimensionality is restricted to nanometer-sized distances in at least one dimension.[5] These are at times called quantum confinement effects.[6] Differences in properties between nanoparticle and bulk metal samples can also arise from so-called surface effects, as described below. It is broadly acknowledged that a fundamental understanding and control of the differences and of their origin could help transform the state-of-the-art in technological fields ranging from energy interconversion to molecular electronics.

Surface effects are prominent in nanostructured materials because of their large ratio of surface-to-bulk atoms. Such effects are expected from a wide range of nanoparticle diameters and may arise from an assortment of phenomena. Because they possess a high percentage of surface atoms, metal nanoparticles may exhibit differences in melting, freezing, and sintering behavior when compared to bulk materials. Metal nanostructures exhibit a range of different shapes,[7−9] as a result of anisotropic growth during their synthesis. Crystalline nanoparticles with specific shapes may also contain preferentially oriented surfaces,[3] i.e., when a specific crystallographic plane from the bulk crystalline structure becomes preferentially exposed at surfaces. Preferentially oriented nanoparticles can exhibit surface properties that are different from those of polycrystalline bulk or polycrystalline nanoparticles but that are relatable, in principle, to the surface properties of well-ordered single crystal surfaces.[8]

[†] Pontifical Catholic University of Puerto Rico.
[‡] University of Alicante.
[§] University of Oviedo.
[II] University of Puerto Rico.

(1) Somorjai, G.; Park, J. *Top. Catal.* **2008**, *49* (3), 126–135.
(2) Somorjai, G.; Tao, F.; Park, J. *Top. Catal.* **2008**, *47* (1), 1–14.
(3) Solla-Gullón, J.; Rodríguez, P.; Herrero, E.; Aldaz, A.; Feliu, J. M. *Phys. Chem. Chem. Phys.* **2008**, *10* (10), 1359–1373.
(4) Rolison, D. R. *Science* **2003**, *299* (5613), 1698–1701.
(5) Ozer, M. M.; Jia, Y.; Zhang, Z.; Thompson, J. R. *Science* **2007**, *316* (5831), 1594–1597.
(6) Shikin, A.; Adamchuk, V. *Phys. Solid State* **2008**, *50* (6), 1170–1185.
(7) Ahmadi, T. S.; Wang, Z. L.; Green, T. C.; Henglein, A.; El-Sayed, M. A. *Science* **1996**, *272* (5270), 1924–1925.
(8) Rodríguez, P.; Herrero, E.; Solla-Gullón, J.; Vidal-Iglesias, F. J.; Aldaz, A.; Feliu, J. M. *Electrochim. Acta* **2005**, *50* (21), 4308–4317.
(9) Hernandez, J.; Solla-Gullón, J.; Herrero, E.; Aldaz, A.; Feliu, J. M. *J. Phys. Chem. C* **2007**, *111* (38), 14078–14083.

Preferentially oriented nanoparticles hold promise as model surfaces for the study of interfacial phenomena at the nanometer scale.

Molecular adsorption at nanostructured metal surfaces already plays an important role in nanoscience. As an enabling technology, surfactant molecules and polymers have been used in colloid chemistry to direct the anisotropic growth of metal nanoparticles during their syntheses[1−3,7] and to prevent agglomeration or sintering of the resulting nanostructures during their use. Organic adlayers have been used to alter the conductive,[10] catalytic,[11,12] and photophysical[13] properties of nanoparticle-derived structures. During the catalytic oxidation of CO over capped Pt nanoparticles, the reaction turnover was reported to vary when the organic capping agents were changed.[11] Hybrid excitation states, which emerge from molecule−plasmon interactions, have been used to influence and control molecular excited states and energy dissipation processes in organic J-aggregates at the surface of gold and silver nanoparticles.[13] The improvement of ohmic contacts has been reported[10] for silver nanoparticles stabilized with oleic acid and subsequently used to print electrical contacts during manufacture of organic thin film transistors (OTFT). The observed performance was superior to other capping agents and was identical to vapor-deposited gold, an industry standard. Control of molecular orientation of aromatic molecules[14−16] at metallic−organic interfaces has been recognized as an important parameter to optimize charge injection in OTFT and in related devices[17] for which well-ordered vertically oriented aromatic molecules are expected to exhibit improved performance. The above examples demonstrate that a fundamental understanding of molecular adsorption at nanoparticle surfaces will play a critical role for attaining the full technological prospects of nanoscience. Toward this end, it seems important to elucidate if preferentially oriented nanoparticles can provide suitable working surfaces to control and to study structure−property relationships emanating from molecular adsorption at nanoparticle surfaces.

Electrochemical methods, in general, are intrinsically sensitive to interfacial structure and composition. Knowledge regarding the specific mode of adsorbate chemisorption and their chemical identity is deemed necessary in order to advance the design of molecular electronic circuits, fuel cells, electrochemical sensors, and electrocatalysts. For this reason, the field of electrochemical surface science,[18] which merges classical electrochemistry[19] and surface science techniques and concepts,[20] has pursued a systematic approach to develop an atomic-level understanding of electron-transfer reactions at model electrode−electrolyte interfaces. As a model system, well-ordered Pt(*hkl*) single crystal surfaces have received considerable attention. However, because many commercial electrocatalysts are in fact metal nanoparticles dispersed and deposited over a conducting porous support, the prospect of fully exploiting possible interrelations between atomic surface structure, composition, and nanoarchitecture, to bring about desired physical and chemical properties, still lays ahead.[4] One requirement is to find suitable systems and methods that can help bridge the existent materials gap between (i) the already abundant literature entailing model experimental and theoretical studies at well-ordered single crystals and (ii) the bourgeoning literature pertaining to nanostructured materials that is not usually focused on surface properties. Electrochemical surface science studies at preferentially oriented nanoparticles should prove critical toward achieving that fundamental objective. Toward that end, this manuscript compares the electrochemically controlled adsorption of hydroquinone-derived adlayers and their reductive desorption from nanometer-sized Pt(111) domains present on the surface (i) of model stepped single-crystal electrodes and (ii) of preferentially oriented Pt nanoparticles.

Because of their well-documented electrochemical reactivity,[21,22] quinones have been used in the past as prototypical redox-active, aromatic chemisorbates.[23−31] Past studies[26,28] have demonstrated that the desorption of hydroquinone-derived adlayers ($Q_{(ads)}$) and their full readsorption can be achieved, in the presence of 2 mM hydroquinone ($H_2Q_{(aq)}$) using 0.5 M H_2SO_4 as supporting electrolyte, by controlling the potential of well-ordered Pt(111) single crystal electrodes, via a redox process consistent with eq 1:

$$\frac{Q_{(ads)}}{Pt(111)} + (z+2)e^- + (z+2)H^+ \xleftrightarrow{Pt(111)} \frac{zH_{(ads)}}{Pt(111)} + H_2Q_{(aq)} \quad (1)$$

where z represents the number of hydrogen atoms adsorbed on the Pt(111) surface domains when the $Q_{(ads)}$ molecule is replaced. This electrochemical behavior is not detected at conventional polycrystalline Pt electrodes,[32] nor at electrochemically disordered Pt(111) single crystal electrodes,[26] nor at ordered Pt(110) or Pt(100),[26,28] so far requiring the presence of massive well-

(10) Wu, Y.; Li, Y.; Ong, B. S. *J. Am. Chem. Soc.* **2006**, *128* (13), 4202–4203.
(11) Park, J. Y.; Lee, H.; Renzas, J. R.; Zhang, Y.; Somorjai, G. A. *Nano Lett.* **2008**, *8* (8), 2388–2392.
(12) Solla-Gullón, J.; Gómez, R.; Aldaz, A.; Pérez, J. M. *Electrochem. Commun.* **2008**, *10* (2), 319–322.
(13) Wiederrecht, G. P.; Wurtz, G. A.; Bouhelier, A. *Chem. Phys. Lett.* **2008**, *461* (4−6), 171–179.
(14) Thayer, G. E.; Sadowski, J. T.; Meyer zu Heringdorf, F.; Sakurai, T.; Tromp, R. M. *Phys. Rev. Lett.* **2005**, *95* (25), 256106.
(15) Anthony, J. E. *Chem. Rev.* **2006**, *106* (12), 5028–5048.
(16) Coropceanu, V.; Cornil, J.; da Silva Filho, D. A.; Olivier, Y.; Silbey, R.; Bredas, J. L. *Chem. Rev.* **2007**, *107* (4), 926–952.
(17) Makinen, A. J.; Long, J. P.; Watkins, N. J.; Kafafi, Z. H. *J. Phys. Chem. B* **2005**, *109* (12), 5790–5795.
(18) Wieckowski, A., Ed. *Interfacial Electrochemistry. Theory, Experiments and Applications*; Marcell Dekker: New York, 1999.
(19) Bard, A. J.; Faulkner L. R. *Electrochemical Methods: Fundamentals and Applications*; 2nd ed.; John Wiley and Sons, Inc.: New York, 2001.
(20) Masel, R. I. *Principles of Adsorption and Reaction on Solid Surfaces*; John Wiley & Sons: New York, 1996.
(21) Patai S., Ed. *The Chemistry of the Quinonoid Compounds*; John Wiley and Sons: New York, 1974; Vol. I.
(22) Patai S., Ed. *The Chemistry of the Quinonoid Compounds*; John Wiley and Sons: New York, 1988; Vol. II.
(23) Inukai, J.; Wakisaka, M.; Yamagishi, M.; Itaya, K. *Langmuir* **2004**, *20* (18), 7507–7511.
(24) Inukai, J.; Wakisaka, M.; Itaya, K. *Chem. Phys. Lett.* **2004**, *399* (4−6), 373–377.
(25) Soriaga, M. P. *Chem. Rev.* **1990**, *90* (5), 771–793.
(26) Rodríguez-López, M.; Herrero, E.; Feliu, J. M.; Tuñón, P.; Aldaz, A.; Carrasquillo, A. *J. Electroanal. Chem.* **2006**, *594* (2), 143–151.
(27) Rodríguez-López, M.; Rodes, A.; Berná, A.; Climent, V.; Herrero, E.; Tuñón, P.; Feliu, J. M.; Aldaz, A.; Carrasquillo, A. *Langmuir* **2008**, *24* (7), 3551–3561.
(28) Rodríguez-López, M.; Rodes, A.; Herrero, E.; Tuñón, P.; Feliu, J. M.; Aldaz, A.; Carrasquillo, A. *Langmuir* **2009**, *25* (17), 10337–10344.
(29) Rodriguez-Lopez, M. Tuñon, P. Feliu, J. M. Aldaz A. and Carrasquillo, Jr, A. *Langmuir* **2010**, *26* (3), 2124−2129.
(30) Chia, V. K. F.; Stickney, J. L.; Soriaga, M. P.; Rosasco, S. D.; Salaita, G. N.; Hubbard, A. T.; Benziger, J. B.; Perter Pang, K. W. *J. Electroanal. Chem.* **1984**, *163* (1−2), 407–413.
(31) Hubbard, A. T. *Chem. Rev.* **1988**, *88* (4), 633–656.
(32) Krauskopf, E. K.; Wieckowski, A. *J. Electroanal. Chem.* **1990**, *296* (1), 159–169.

ordered Pt(111) single-crystal surfaces in order to be detected.[26,28] Those studies suggest the possibility of employing the differences in electrochemical reactivity exhibited by hydroquinone-derived adlayers (i) as part of an electroanalytical scheme to verify the existence of well-ordered Pt(111) domains and/or (ii) as electrochemically controlled aromatic molecular barriers, capable of selectively capping or decapping nanometer-sized Pt(111) domains by suitable control of an external stimuli such as the applied potential. In this manuscript, stepped Pt(*hkl*) single-crystal electrode surfaces are used as model systems in which the dimensionality and the surface density of available well-ordered Pt(111) domains, present as terraces, can be restricted and controlled experimentally. In this way, model dimensionally restricted hydroquinone-derived adlayers, i.e., $Q_{(ads)}$ on Pt(111) domains at terraces, are synthesized and studied. The results obtained at the stepped Pt(*hkl*) surfaces suggest that in the presence of 2 mM $H_2Q_{(aq)}$ the electrochemically detected desorption−adsorption process, ascribed to eq 1, takes place selectively from ordered Pt(111) domains present as terraces. This domain-selective electroanalytical detection scheme is employed later to selectively monitor desorption−adsorption of hydroquinone-derived adlayers from ordered, nanometer-scaled Pt(111) domains on the surface of preferentially oriented Pt nanoparticles, confirming the existence of such well-ordered (111) domains on the surface of the Pt nanoparticles. The ability of the molecular adlayers to selectively preclude the electrochemical reactivity expected between nanoparticle surface sites and electrolyte components is demonstrated by use of CO-displacement experiments.

2. Experimental Section

Pt nanoparticles deposited on suitably clean Au substrates have been used in this work. Au was selected as a substrate because it can be conveniently cleaned, and it does not contribute significantly to the measured currents in the range of potentials of interest. Preferentially oriented Pt nanoparticles were prepared by using the so-called colloidal method.[3] Briefly here, a variable amount of sodium polyacrylate (PA) solution was added to 100 mL of an aged 10^{-4} M solution containing the desired Pt precursor. K_2PtCl_4 was employed for the synthesis of samples containing large (100) domains ($_{nano}Pt_{(100)}$) whereas H_2PtCl_6 was used for the samples containing large (111) domains ($_{nano}Pt_{(111)\text{-}(100)}$ and $_{nano}Pt_{(111)\text{-}(110)}$). After 20 min of Ar bubbling, the Pt ions were reduced by bubbling H_2 for 5 min. The reaction vessel was then sealed, and the solution was left overnight. Once the Pt has been completely reduced (12−24 h), two NaOH pellets were added to produce the full precipitation of the nanoparticles. Then, the nanoparticles were washed 3−4 times with ultrapure water. The particle size and morphology of the nanoparticle samples were characterized by transmission electron microscopy (TEM).[3]

The cleaning of the Pt nanoparticles after preparation is a crucial step in the process and uses $CO_{(g)}$ as a displacing ligand to forcibly remove foreign species from the electrode surface.[3] Classical electrochemical procedures to decontaminate platinum by electrochemical cycling cannot be used because high anodic potential limits must be avoided to preserve the surface order of the synthesized nanoparticles. It is well established that surface perturbations induced by CO cleaning are minor when compared to electrochemical oxygen adsorption.[33,34] Aqueous 0.5 M H_2SO_4 solutions were used as supporting electrolyte throughout the voltammetric study. They were prepared from concentrated sulfuric acid (Merck Suprapur or Aldrich Teflon grade) and Purelab Ultra (Elga-Vivendi) water (18 MΩ cm). This electrolyte is more convenient than other choices because the adsorption states at well-ordered Pt(*hkl*) surfaces have been thoroughly studied and are well-defined voltammetrically. Coulometry measurements derived from voltammetry, in the hydrogen/anion adsorption region, were used to determine the real surface area of each sample studied. A value of 210 $\mu C \cdot cm^{-2}$ is conventionally assumed throughout. High purity materials were used to safeguard nanoparticle cleanliness and system composition. Furthermore, the magnitude, sharpness, symmetry, and reproducibility of cyclic voltammetry peaks were also used to evaluate and monitor the presence or absence of surface contamination, i.e., CV analysis was the starting point of each of the experiments reported at $_{nano}$Pt samples.

Pt(*hkl*) single crystal electrode surfaces were prepared using the procedures developed by Clavilier et al.[35] Prior to any experiment, Pt(*hkl*) single crystal surfaces were flame-annealed and cooled in an atmosphere of argon/hydrogen. An EG&G PAR Model 175 Universal Programmer, an AMEL 551 potentiostat, a Soltec XY recorder, and an eCorder401 (eDAQ, Australia) were used in the voltammetric experiments for the Pt(*hkl*) electrodes. For the Pt nanoparticles, an Autolab PGSTAT30 equipped with an analog scan generator was used (Ecochemie, Utrecht, Netherlands). Platinum counter electrodes were used throughout the study, and all potentials were measured and are reported versus the reversible hydrogen electrode (RHE) with the same supporting electrolyte solution. The RHE was contained in a separate compartment from the working electrode with contact made through a Luggin capillary. All experiments were conducted at room temperature, 25 °C (±2 °C). H_2Q was obtained from Aldrich and used as received. High purity gases (5N) were used.

3. Results and Discussion

3.1. CV Characterization of Pt(*hkl*) Single-Crystal Electrodes Having Stepped Surfaces Vicinal to the Pt(111) Basal Plane and of Their Reactivity Toward Oxidative-Chemisorption/Reductive-Desorption of Hydroquinone-Derived Adlayers. In the past, electrochemical surface science studies have relied predominantly on the use of basal Pt(*hkl*) single crystal electrode surfaces. Increasingly, vicinal surfaces have proven useful[17,36−39] (i) to confirm reactivity trends predicted from studies performed at basal (111), (110), or (100) planes, as well as (ii) to model the role played by defects in determining the overall surface reactivity in nonmodel systems. In this study, vicinal surfaces are tailored to contain a choice of Pt(111) terrace dimensions combined with monatomic steps of (110) symmetry. The Miller indexes defining the vicinal crystallographic planes have values Pt(n,n,n − 2), where n defines the number of atomic rows in the terraces. The resulting surfaces can conveniently be referred as belonging to the stepped series Pt(S)[(n)(111)×(111)]. However, as the junction of a (111) terrace site and a (111) step site define a (110) step site, the series can alternatively be described as Pt(S)[(n − 1)(111)×(110)], which better describes the electrochemical behavior of these electrodes.

Figure S1 (Supporting Information) shows CV experiments collected using well-ordered Pt(*hkl*) single crystal electrodes immersed in 0.5 M H_2SO_4 supporting-electrolyte solutions. The

(33) Itaya, K.; Sugawara, S.; Sashikata, K.; Furuya, N. *J. Vacuum Sci. Technol., A* **1990**, *8* (1), 515–519.
(34) Zurawski, D.; Rice, L.; Hourani, M.; Wieckowski, A. *J. Electroanal. Chem. Interfacial Electrochem.* **1987**, (1−2), 221–231.
(35) Clavilier, J.; El Achi, K.; Petit, M.; Rodes, A.; Zamakhchari, M. A. *J. Electroanal. Chem.* **1990**, *295*, 333–356.
(36) Lebedeva, N. P.; Koper, M. T. M.; Feliu, J. M.; van Santen, R. A. *J. Phys. Chem. B* **2002**, *106* (50), 12938–12947.
(37) Motoo, S.; Furuya, N. *Ber. Bunsen-Ges.* **1987**, *91*, 457–461.
(38) Buller, L. J.; Herrero, E.; Gómez, R.; Feliu, J. M.; Abruña, H. D. *J. Phys. Chem. B* **2000**, *104* (25), 5932–5939.
(39) Maciá, M. D.; Herrero, E.; Feliu, J. M. *Electrochim. Acta* **2002**, *47* (22−23), 3653–3661.

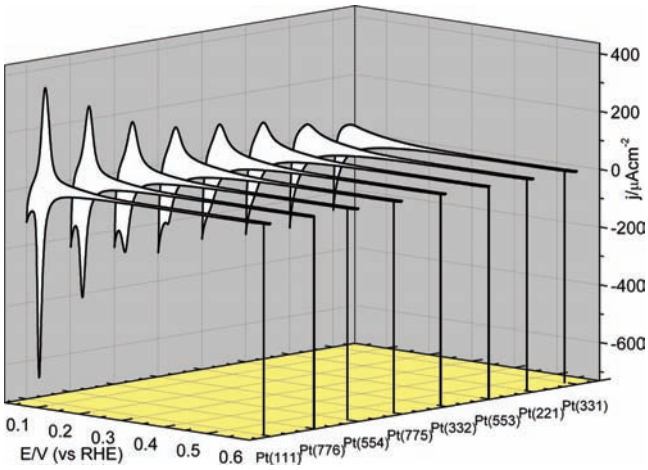

Figure 1. CVs of well ordered Pt(S)[(n − 1)(111)×(110)] stepped surfaces electrodes collected in 2 mM H_2Q + 0.5 M H_2SO_4. Scan rate 50 mV s^{-1}. Temp 25 °C.

initial structure of each Pt(*hkl*) electrode was evaluated using these CV experiments. They each served as the starting point of the experiments shown in Figure 1. The first voltammogram in Figure S1, for example, shows the now familiar shape of the CV for a clean, well-ordered Pt(111) single crystal electrode surface in clean 0.5 M H_2SO_4. As reported previously by Clavilier,[35] the CV should (i) be reproducible and stable upon repetitive cycling, (ii) contain reversible anodic and cathodic features that exhibit (iii) a near featureless hydrogen UPD region from 0.3 V onto more negative potentials with (iv) a sharp spike at ca. 0.45 V, which overlaps (v) the (bi)sulfate adsorption contribution from ca. 0.3 to 0.5 V. The onset of the hydrogen evolution reaction (HER) takes place at more negative potentials, beginning at ca. 0.08 V. The additional CV experiments in Figure S1, were collected applying identical experimental conditions but using well-ordered Pt(n,n,n − 2) single crystal surfaces in 0.5 M H_2SO_4 supporting electrolytes. Several important trends in the CV responses are noted in the series. Three aspects are emphasized herein due to their relevance to this report. (i) The CV feature ascribed to (bi)sulfate adsorption/desorption on Pt(111), ca. 0.3 to 0.5 V, exhibits a trend toward more positive potentials with diminishing values of n while exhibiting smaller absolute charge densities. The feature exhibits a trend toward vanishing as n approaches zero, through the CV experiments at the series of Pt(S)[(n − 1)(111)×(110)] electrodes. The decrease in current density of the (bi)sulfate adsorption/desorption CV feature has been associated to the decrease in surface density of Pt(111) domains expected at the Pt(S)[(n − 1)(111)×(110)] series, i.e., increasing the surface density of Pt(110) steps in the vicinal surface decreases the availability of ordered Pt(111) domains. (ii) A second important trend in the CV curves is the noticeable increase in the current densities within the potential region near 0.1 V. The redox feature emerging near this potential is associated with H as well as anion adsorption at Pt(110) step defects.[40−42] Figure S0

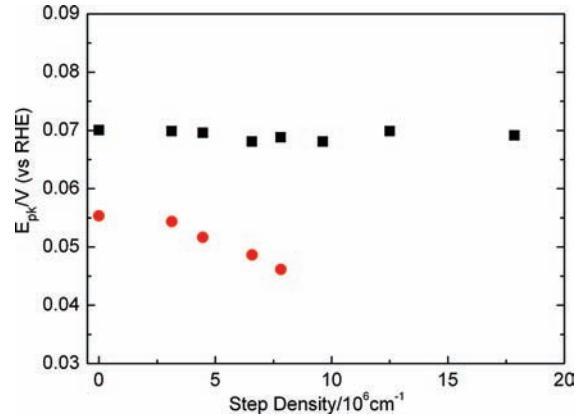

Figure 2. Peak potentials (E_{pk}) as a function of the surface step density, for the anodic (black square) and cathodic (red circles) branches, obtained from the CVs of the Pt(S)[(n − 1)(111×110)] electrodes in 2 mM H_2Q + 0.5 M H_2SO_4. All other conditions as in Figure 1.

(Supporting Information) may be used as a visual reference. To a first approximation, the 2D Pt(111) terraces in the Pt(S)[(n − 1)(111)×(110)] electrode surfaces may be assumed to be well-ordered domains,[43] very large (formally ∼ ∞) in one dimension and dimensionally restricted in the other direction, as defined by the step-to-step distance. The actual width of the terraces (n − 5/3)d($3^{1/2}$/2) varies from 0.32 to 2.96 nm for n = 3 to n = 14, respectively, where d is the metallic radii of Pt. The expected Pt(110) step density may be calculated, for this vicinal series, by using eq 2:

$$\text{step density} = \frac{1}{\frac{\sqrt{3}}{2}d\left(n - \frac{2}{3}\right)}\ \text{cm}^{-1} \qquad (2)$$

A detailed discussion of the hard-sphere model used to obtain this relation may be found elsewhere.[42−44]

After characterization, each clean, ordered Pt(*hkl*) single crystal electrode was transferred into a 0.5 M H_2SO_4 supporting-electrolyte solution containing 2 mM $H_2Q_{(aq)}$ and equilibrated for 5 min at the initial potential, ca. 0.6 V, to produce Pt(*hkl*) electrodes fully coated with $Q_{(ads)}$. At this potential, the oxidative chemisorption of hydroquinone is known to take place at Pt(111)[26] and is also expected at Pt(110) and Pt(100) surfaces.[28] After equilibration of the electrodes in the 2 mM $H_2Q_{(aq)}$ solution, the electrodes were cycled until a steady voltammogram was achieved, Figure 1. The voltammograms in Figure 1 show a redox pair at ca. 0.06 V, which is the process of interest in this study. It is ascribed to the process in eq 1, which has been discussed in detail elsewhere.[26−28] Briefly here, some aspects of the CV reveal the formation of a compact, full monolayer of $Q_{(ads)}$ on the Pt(111) surface upon exposure to the 2 mM $H_2Q_{(aq)}$ solution. The first is the complete disappearance of the sulfate adsorption, of the spike and of the hydrogen UPD characteristic of clean Pt(111) electrodes. The second is the appearance of the redox process, centered at ca. 0.06 V, due to hydrogen-assisted reductive desorption of $Q_{(ads)}$ and to the oxidative readsorption of $H_2Q_{(aq)}$ present in the vicinity of

(40) Al-Akl, A.; Attard, G. A.; Price, R.; Timothy, B. *J. Electroanal. Chem.* **1999**, *467* (1−2), 60–66.
(41) Gómez, R.; Climent, V.; Feliu, J. M.; Weaver, M. J. *J. Phys. Chem. B* **2000**, *104* (3), 597–605.
(42) Clavilier, J. Electrochemical Surface Characterization of Platinum Electrodes Using Elementary Electrosorption Processes at Basal and Stepped Surfaces. In *Electrochemical Surface Science: Molecular Phenomena at Electrode Surface*; Soriaga, M. P., Ed.; American Chemical Society: Washington, DC, 1988; pp 202−215.
(43) Clavilier, J.; El Achi, K.; Rodes, A. *Chem. Phys.* **1990**, *141* (1), 1–14.
(44) Rodes, A. A Molecular Approach to the Study of Electrode Processes: Electrochemical Characterization of Platinum Stepped-Surfaces and Their Application to the Study of Surface Reconstruction Processes. Ph.D. Thesis, 1991, University of Alicante, Spain.

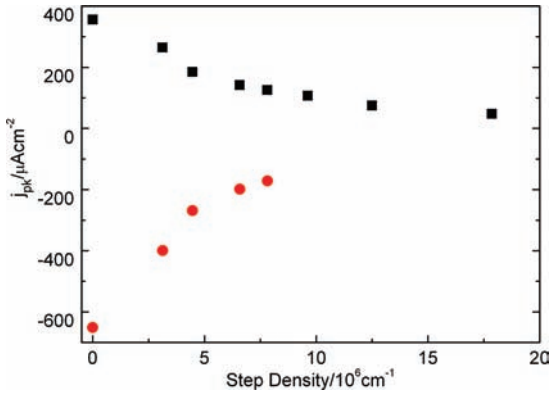

Figure 3. Peak current densities as a function of the surface step density, for the anodic (black square) and cathodic (red circles) branches, obtained from the CVs of Pt(S)[$(n-1)(111)\times(110)$] stepped surfaces in 2 mM H_2Q + 0.5 M H_2SO_4. All conditions as in Figure 1.

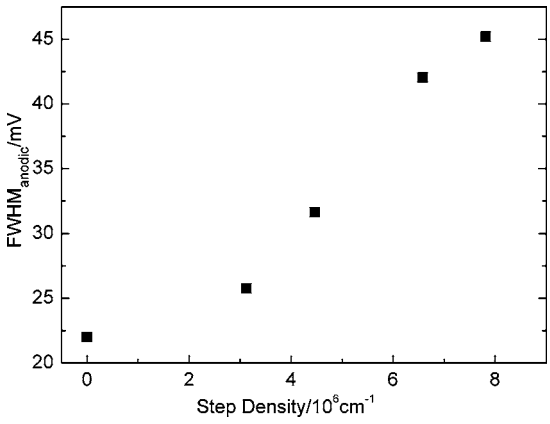

Figure 4. FWHM as a function of the surface step density, for the anodic branch, obtained from the CVs of the Pt(S)[$(n-1)(111\times110)$] stepped surface electrodes in 2 mM H_2Q + 0.5 M H_2SO_4. All conditions as in Figure 1.

the electrode.[26,28] It is important to bear in mind during the ensuing discussion that this process has only been reported, so far, at well-ordered Pt(111) electrodes and it is not observed at the other basal planes, i.e., Pt(100) or Pt(110).[28] The peak potentials, peak current densities, and FWHM from the CV experiments performed in presence of 2 mM $H_2Q_{(aq)}$ in 0.5 M H_2SO_4 supporting electrolyte (Figure 1), measured for each of the individual Pt(S)[$(n-1)(111)\times(110)$] electrodes, are presented in Figure 2, Figure 3, and Figure 4, respectively.

The peak potentials, E_{pk} (V), from the CV experiments in Figure 1, are represented in Figure 2 as a function of the Pt(110) step density in the series. Note that the anodic branch, $_aE_{pk}$, remains constant and only small variations in peak potential are measured as a function of terrace size, $_aE_{pk} = 0.069$ V($\pm$0.002), within the experimental accuracy and precision. In contrast, the cathodic branch, $_cE_{pk}$, trends toward less positive values, within the range 0.046 V $\leq {}_cE_{pk} \leq$ 0.055 V, as the step density increases, i.e., with diminishing terrace sizes. An increase in the relative contribution of background processes to the total current could account for this shift, i.e., the effect could be due to an overlap with the onset of the hydrogen evolution reaction (HER), which should have a larger effect on the cathodic branch, as observed. Also, because the Pt(110) step sites do remain covered by the hydroquinone-derived adlayer[28] through the voltammetry experiments (vide infra), it is reasonable to consider that the free energy and/or kinetics of desorption from Pt(111) terraces could be influenced by the presence of the irreversibly adsorbed molecules at the Pt(110) step sites. Yet an additional possibility is that the desorption process at (111) terraces could be influenced by changes in the potential of zero total charge (pztc), which shifts to lower values as the density of steps is increased.[45]

The peak current density, j_{pk} (A cm^{-2}), has been selected as an experimental parameter of interest because, for isolated noninteracting redox centers, it is proportional to the concentration of electroactive species.[19] Figure 3 shows the peak current densities for both the anodic and the cathodic processes. The peak current density, for each Pt(n,n,$n-2$) sample electrode, is plotted as a function of the step density. A decrease in absolute peak current density is observed as the density of Pt(110) steps increases. Note that an increase in Pt(110) step density necessarily results in a concomitant decrease in the availability of Pt(111) surface sites per unit surface area. The observed trend, i.e., a decrease in absolute current density as a function of Pt(110) step density, is consistent with a surface process that is precluded at the Pt(110) steps but that continues to take place at the available well-ordered Pt(111) domains, i.e., surface terraces. Note also that the oxidation process can be detected even under conditions of restricted terrace dimensionality, in this case near the quasi 1D limit. The general trend is important because it suggests that, under these experimental conditions, the process ascribed to eq 1 behaves as a domain-selective process. The current densities, however, do not decrease linearly with step density. This is primarily due to the role of lateral interactions, as described in the discussion of Figure 4 and Figure S2. It is also caused by the residual contribution to the total absolute current density expected, for both the cathodic and anodic branches, due to processes associated with the presence of the irreversibly adsorbed molecular adlayer which remains present at the Pt(110) step sites.[28] Nonzero current densities were previously reported, near this potential region, at quinone-coated Pt(110) single crystal electrodes treated with hydroquinone.[28]

Figure 4 compares the FWHM for the anodic peaks, represented here versus the Pt(110) step density. Anodic peaks were selected because they tend to be more symmetric than the cathodic peaks, presumably due to the negligible extent of interference from the hydrogen oxidation reaction (HOR). In Figure 4, the FWHM trend toward higher values as a function of the step density, and a range of values from 22.0 mV to 45.2 mV was measured. For an ideal nernstian reaction under Langmuir isotherm conditions, the FWHM is expected to be (90.6/n)mV.[19] In classic molecular adsorption models,[46] the observation of peaks narrower than (90.6/n)mV is usually ascribed to attractive interaction within the adlayer.[47] The changes in FWHM are important because they could influence peak morphology and, concomitantly, absolute peak current densities. Despite these noted caveats, the correlation established in Figure 3 does support the viability of using the process ascribed to eq 1, under controlled conditions, as an electroanalytical indicator signaling the availability of well-ordered Pt(111) surface domains.

If interferences can be avoided, a more robust correlation could be expected between the charge density and the surface density of well-ordered Pt(111) domains, which should be

(45) Climent, V.; García-Aráez, N.; Herrero, E.; Feliu, J. *Russian J. Electrochem.* **2006**, *42* (11), 1145–1160.
(46) Srinivasan, S.; Gileadi, E. *Electrochim. Acta* **1966**, *11* (3), 321–335.
(47) Laviron, E. *J. Electroanal. Chem.* **1974**, *52* (3), 395–402.

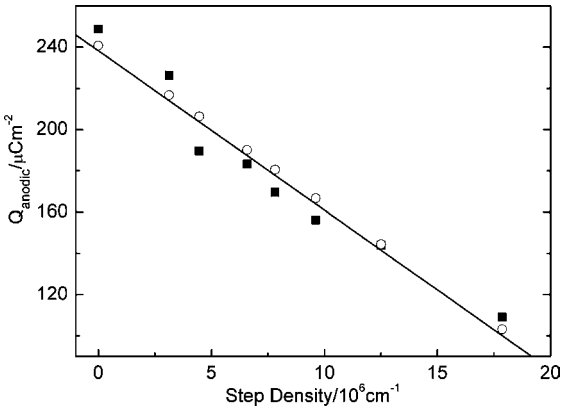

Figure 5. Total charge density (Q_{total}) under the anodic peaks (squares) as a function of surface step density obtained during the CV experiments in Figure 1. The linear regression (solid line) is shown for reference. Theoretical charge (open circles) for a redox process selective to Pt(111) terrace atoms; one electron per Pt(111) terrace atom is assumed.

relatable coulometrically via the domain-selective redox process in eq 1. Because of the known caveats affecting the cathodic branch, the anodic branch was selected to perform the coulometry analysis. Figure 5 compares the total charge density that was obtained from the anodic branch of the CV at potentials extending from 0.035 to 0.33 V. These are presented, without corrections, versus the Pt(110) step density. A reasonable degree of correlation is obtained with the best-fit trend line, shown for reference in Figure 5. Also shown for reference is the theoretical charge (open circles) expected for a domain-selective redox process, assuming a faradaic equivalency of one electron per Pt(111) terrace atom. To a first approximation, the coulometry results confirm that, under well-controlled experimental conditions, the process ascribed to eq 1 does behave as a domain-selective molecular surface probe which signals changes in availability of well-ordered Pt(111) surface domains. In the next section, this domain-selective electrochemical reaction is used to monitor desorption−adsorption of hydroquinone-derived adlayers from ordered, nanometer-scaled Pt(111) domains on the surface of preferentially oriented Pt nanoparticles.

On the basis of results at the basal planes,[28] at these vicinal surfaces, the reductive desorption is expected to take place from Pt(111) terraces while Pt(110) step-sites should remain covered by the adsorbed molecules. This expectation is confirmed in Figure S2, Supporting Information. The CV experiment (nine cycles), shown as solid lines in Figure S2, was performed in clean supporting electrolyte after (i) removing a quinone-coated Pt(554) electrode, prepared by exposure to a 0.5 M H_2SO_4 + 2 mM $H_2Q_{(aq)}$ solution, and subsequently (ii) rinsing the electrode with clean supporting electrolyte solution to prevent transfer of $H_2Q_{(aq)}$ to the test cell. The arrows highlight the observed trend, i.e., a decrease in the process at ca. 0.06 V and a concomitant reappearance of features in the range of potentials associated to hydrogen UPD and (bi)sulfate adsorption at Pt(111) domains. For reference, the CV response for the clean and ordered Pt(554) electrode is also shown (dotted line). Three important observations are associated to the presence of irreversibly adsorbed molecules at the step sites: (i) Even after nine cycles, no recovery of the Pt(110) sites is detected, i.e., the redox feature near 0.1 V is not recovered. This observation confirms the presence of adsorbed molecules at Pt(110) step sites. (ii) Overall recovery of (111) domains is lower at this stepped surfaces than previously reported for defect-free Pt(111) electrodes.[26] (iii) Recovery is better for the hydrogen UPD features than for the (bi)sulfate feature. These last two observations suggest a higher specificity for sulfate adsorption than for H adsorption, and the existence of interactions between the molecules nominally occupying the Pt(110) step sites and those at the Pt(111) terrace sites.

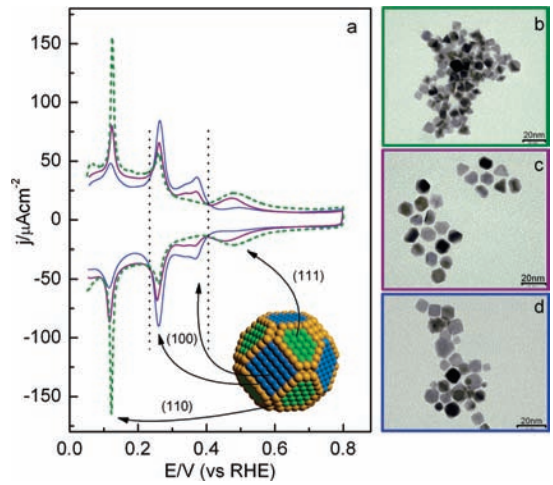

Figure 6. (a) Steady CVs of three clean Pt nanoparticle samples collected in 0.5 M H_2SO_4 supporting electrolyte: (i) thick dashed line (green) for $_{nano}Pt_{(111)-(110)}$, (ii) medium-thickness solid line (purple) for $_{nano}Pt_{(111)-(100)}$, and (iii) thin solid line (blue) for $_{nano}Pt_{(100)}$. Scan rate 50 mV s^{-1}. Temp. 25 °C. TEM images of (b) $_{nano}Pt_{(111)-(110)}$ sample, (c) $_{nano}Pt_{(111)-(100)}$ sample, (d) $_{nano}Pt_{(100)}$ sample.

3.2. Characterization of Preferentially Oriented Pt Nanoparticles and Electrochemical Reactivity of Hydroquinone-Derived Adlayers at $_{nano}$Pt Electrode Surfaces. Three different samples of preferentially oriented Pt nanoparticles were used in this study. They were prepared by variations of the colloid chemistry synthesis method, i.e., using sodium polyacrylate as a capping agent. The method produces different shapes of nanoparticles as a function of the experimental conditions used during synthesis. TEM images for these three samples are observed in the right-hand panel of Figure 6. TEM measurements can provide quantitative information about the average size and the relative size distribution of the nanoparticles within a given sample. Qualitative information can also be derived from the images such as the predominant shape of the nanostructures present in the sample. The first TEM image (top) corresponds to the sample $_{nano}Pt_{(111)-(110)}$. TEM measurements (200 particles) reveal an average size of 8.6 ± 1.4 nm. Pt nanoparticles with preferential octahedral and triangular shapes can be observed in the sample. These shapes have been experimentally associated in the past to the presence of preferentially oriented (111) domains at the surface of the Pt nanoparticles prepared by this method. The next TEM image (middle) corresponds to the sample $_{nano}Pt_{(111)-(100)}$. TEM measurements (121 particles) suggest an average size of 10.3 ± 1.9 nm. Pt nanoparticles with preferential hexagonal and triangular shapes are frequently observed in this sample. Such 2D hexagonal projections have been related empirically with the coexistence of (111) and (100) surface domains in 3D cubooctahedral nanoparticles.[1] The last TEM image (bottom) corresponds to the sample $_{nano}Pt_{(100)}$. TEM measurements reveal an average size of 8.2 ± 1.6 nm (142 particles). Cube-shaped Pt nanoparticles, associated to preferentially oriented (100) surface domains, are observed with higher frequency in this sample.

Table 1 summarizes the relative % of Pt(111) and Pt(100) surface sites present at each of the nanoparticle samples used

Table 1. Fraction of the Pt(111) and Pt(100) Ordered Domains Determined for the Different Nanoparticles

sample	(111) sites/%	(100) sites/%
$_{nano}Pt_{(111)-(110)}$	42	3
$_{nano}Pt_{(111)-(100)}$	30	32
$_{nano}Pt_{(100)}$	18	40

in this study. The measurements in Table 1 were performed using an in situ electrochemical characterization method based on oxidation of adsorbed Bi or Ge. The UPD processes of Bi and Ge have been used in the past to quantify the number of Pt(111) and Pt(100) surface sites, respectively[3,8,48,49] The electrochemical methods are complementary with characterization by high resolution TEM (HRTEM) because they are less time-consuming and provide in situ, surface sensitive information about all the electrochemically active surface sites available during a given experiment. In contrast, HRTEM can provide surface-sensitive structural information but only after evaluating images one nanoparticle at a time.

Figure 6 shows three important reference CV experiments. Each CV was obtained after supporting a different sample of Pt nanoparticles onto a previously cleaned Au substrate, such that the Pt nanoparticles act as the active electrode surface ($_{nano}$Pt) during the experiment. Prior to collecting each CV, the $_{nano}$Pt electrodes were cleaned according to the method described in the literature. In brief, each $_{nano}$Pt electrode was analyzed by CV in clean 0.5 M H_2SO_4 within a range of potentials in which the surface order of the electrode is preserved. Each $_{nano}$Pt electrode was then subjected to CO adsorption/oxidation until a clean and reproducible CV was obtained. Each CV in Figure 6 was then collected in clean supporting electrolyte.

The clean cyclic voltammograms, shown in Figure 6, were collected at the beginning of each of the three experiments discussed further in Figures 7, 8, S3, 9. The initial steady voltammograms (Figure 6) serve several purposes. First, the peak symmetry provides a qualitative measure of initial surface and overall system cleanliness. Second, in the case of clean Pt samples, the overall hydrogen and anion adsorption charge is directly proportional to the amount of surface Pt atoms. Hence, the integrated charge obtained from the CV in clean supporting electrolyte can be used to calculate the real surface area for the clean Pt surfaces. Third, the relative distribution of charge among the voltammetic peaks provides an estimate of the relative distribution of electrochemically available surface sites on the $_{nano}$Pt electrode surface, such as (111) sites, (100) sites, (110) sites, etc.[3] Note, for example, the presence of two isopotential points, the first at ca. 0.24 V and the second at ca. 0.4 V. These arise as a consequence of differences in the relative surface concentration of Pt(*hkl*) sites and domains in each of the $_{nano}$Pt samples. Pt(*hkl*) sites and surface domains exhibit characteristic contributions (see Figure S0) to the overall current density as a function of potential: (i) Pt(110) sites are expected to show maximum contributions to the overall current density at ca. 0.12 V; (ii) Pt(100) step sites and Pt(100) terraces show maximum contributions at ca. 0.26 V and 0.37 V, respectively; (iii) ordered Pt(111) surface sites contribute evenly to the range spanning negative from 0.33 V. Pt(111) sites also contribute in the region positive from 0.4 V, with a maximum near 0.5 V,

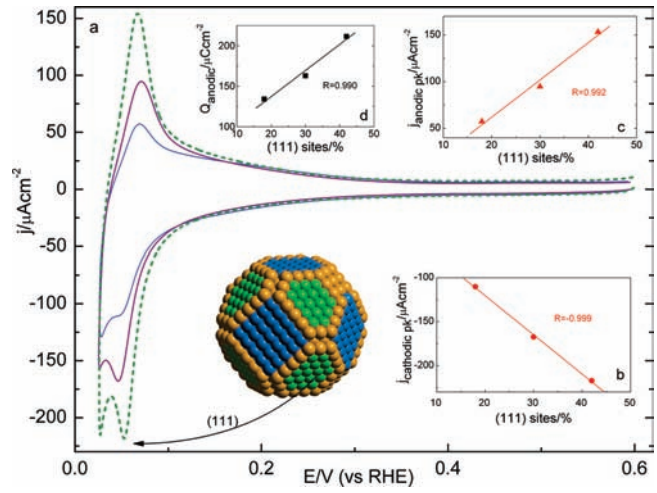

Figure 7. (a) Steady CV of Pt nanoparticle samples in 2 mM H_2Q + 0.5 M H_2SO_4 solution: (i) thick dashed line (green) for $_{nano}Pt_{(111)-(110)}$, (ii) medium-thickness solid line (purple) for $_{nano}Pt_{(111)-(100)}$, and (iii) thin solid line (blue) for $_{nano}Pt_{(100)}$. Scan rate 50 mV s^{-1}. Temp 25 °C. Insets show (b) the cathodic peak current densities, (c) the anodic peak current densities, and (d) the total anodic charge densities as a function of the density of Pt(111) surface sites, expressed as a percent of the electrochemically available surface in each sample.

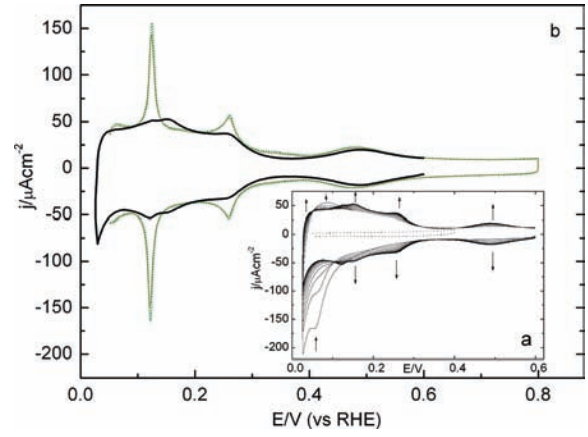

Figure 8. (a) Consecutive CVs of quinone-coated $_{nano}Pt_{(111)-(110)}$ electrode, in 0 mM H_2Q + 0.5 M H_2SO_4, obtained after removal from a 2 mM H_2Q solution: (i) 1st thru 10th CV of the sample, solid line (—) and (ii) steady CV for the CO-coated $_{nano}Pt_{(111)-(110)}$ electrode, dotted line (····). (b) Expanded comparison of CVs: (i) for clean $_{nano}Pt_{(111)-(110)}$ electrode, dotted line (····); (ii) for partly quinone-coated $_{nano}Pt_{(111)-(110)}$ electrode obtained after ten CV cycles in 0.5 M H_2SO_4, thick solid line; (iii) for the recovered $_{nano}Pt_{(111)-(110)}$ electrode after CO adsorption/oxidation cycle, thin solid line. Scan rate 50 mV s^{-1}. Temp 25 °C.

due to the frequently called "unusual adsorption states", which are associated to (bi)sulfate adsorption at Pt(111). Importantly, the decrease in current density at 0.5 V follows the order $_{nano}Pt_{(111)-(110)}$ > $_{nano}Pt_{(111)-(100)}$ > $_{nano}Pt_{(100)}$ and suggests a decrease in the availability of Pt(111) domains,[3] supported in Table 1. A similar conclusion may be reached for the availability of Pt(110) sites by evaluation of the current density at ca. 0.12 V which decreases in the same order. In contrast, notice the concomitant increase in current densities within the range from 0.25 V to 0.4 V, that now increases in the order $_{nano}Pt_{(111)-(110)}$ < $_{nano}Pt_{(111)-(100)}$ < $_{nano}Pt_{(100)}$, giving rise to the aforementioned isopotential points. The increase in current density from 0.25 V to 0.4 V is attributed to an increase in available Pt(100) sites. A good analytical agreement exists between the TEM characterization and the in situ electrochemical characterization

(48) Solla-Gullón, J.; Vidal-Iglesias, F. J.; Rodriguez, P.; Herrero, E.; Feliu, J. M.; Clavilier, J.; Aldaz, A. *J. Phys. Chem. B* **2004**, *108* (36), 13573–13575.
(49) Rodríguez, P.; Solla-Gullón, J.; Vidal-Iglesias, F. J.; Herrero, E.; Aldaz, A.; Feliu, J. M. *Anal. Chem.* **2005**, *77* (16), 5317–5323.

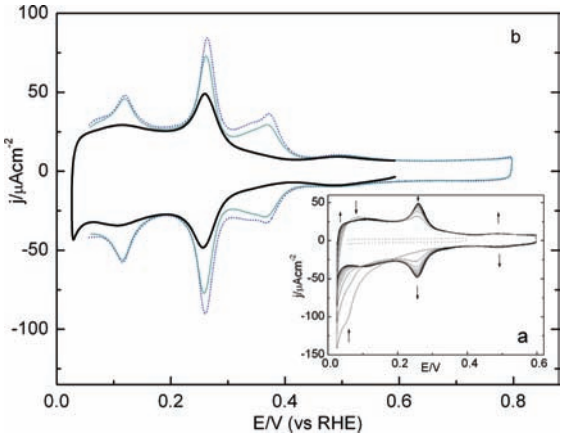

Figure 9. (a) Consecutive CVs of quinone-coated $_{nano}Pt_{(100)}$ electrode, in 0 mM H_2Q + 0.5 M H_2SO_4, obtained after removal from a 2 mM H_2Q solution: (i) 1st thru 10th CV of the sample, solid line (—) and (ii) steady CV for the CO-coated $_{nano}Pt_{(100)}$ electrode, dotted line (····). (b) Expanded comparison of CVs: (i) for clean $_{nano}Pt_{(100)}$ electrode, dotted line (····); (ii) for partly quinone-coated $_{nano}Pt_{(100)}$ electrode obtained after ten CV cycles in 0.5 M H_2SO_4, thick solid line; (iii) for the recovered $_{nano}Pt_{(100)}$ electrode after CO adsorption/oxidation cycle, thin solid line. Scan rate 50 mV s^{-1}. Temp 25 °C.

methods, i.e., the quantitative methods based on oxidation of adsorbed Bi or Ge adatoms and the qualitative surface analysis afforded by the clean cyclic voltammograms. All suggest that the percentage of ordered Pt(111) surface domains decreases in the order $_{nano}Pt_{(111)-(110)} > {}_{nano}Pt_{(111)-(100)} > {}_{nano}Pt_{(100)}$.[3]

After characterization, each clean $_{nano}$Pt electrode was transferred into a 0.5 M H_2SO_4 supporting-electrolyte solution containing 2 mM $H_2Q_{(aq)}$ and equilibrated for 5 min at the initial potential of 0.6 V. Each electrode was then cycled in the hydroquinone-containing solution until a steady voltammogram was produced (15 cycles). The resulting voltammograms are compared in Figure 7. Two relevant aspects are the disappearance of the clean surface features and the observation of a new redox pair at ca. 0.06 V, as observed with the single crystal electrodes. The pair at ca. 0.06 V is assigned to the reductive-desorption and oxidative-chemisorption process, depicted in eq 1, taking place selectively at well-ordered Pt(111) domains present on the surface of the platinum nanoparticles. This assignment can be tested by comparing the peak current density, for the process at ca. 0.06 V, to the density of Pt(111) sites, as previously determined using the independent electrochemical method involving Bi UPD and expressed as a percent of the electrochemically active surface sites in each nanoparticle sample (see Table 1). The comparisons are shown in the insets in Figure 7, for both the cathodic (Figure 7b) and anodic (Figure 7c) branches. A positive correlation exists between the absolute peak current density and the surface density of Pt(111) sites. A positive correlation also exists between the charge density (Figure 7c) of the anodic process and the density of Pt(111) sites. The correlations strongly suggest that the assignment is correct. As will be discussed below, see Figure 8, Figure S3 (Supporting Information), and Figure 9, the electrochemical behavior observed after transfer of the quinone-coated $_{nano}$Pt electrodes to hydroquinone-free supporting electrolyte solutions, is also consistent with this assigment (vide infra).

It is worth summarizing that (i) at the initial potential, 0.6 V, of the experiments in Figure 7, all surfaces on the $_{nano}$Pt samples are totally capped by a full compact layer of $Q_{(ads)}$ at the $_{nano}$Pt surface. This may be deduced from the total disappearance of the voltammetric features expected at the clean $_{nano}$Pt surfaces, i.e., anion and hydrogen adsorption. (ii) At potentials negative of the cathodic peak, well-ordered Pt(111) domains are selectively decapped via the reductive desorption process in eq 1.[28,29] During the positive going scan, (iii) the well-ordered Pt(111) domains are recapped by the reverse process, i.e., oxidative-chemisorption, giving rise to the redox pair at ca. 0.06 V. Throughout the voltammetric experiments, (iv) no evidence for recovery of Pt(110) nor Pt(100) sites or domains is observed, when experiments are performed in presence of 2 mM hydroquinone solutions. These results are consistent with the results obtained at model single crystal surfaces vicinal to the Pt(111) plane and with expectations borne out of previous spectroelectrochemical studies using Pt(111),[26,28,29] as well as Pt(110) and Pt(100), single crystal electrodes.[28]

Figure 8, Figure S3, and Figure 9 show the electrochemical behavior of the quinone-coated $_{nano}$Pt electrodes after transfer to hydroquinone-free supporting electrolyte solutions. Figure 8 relates to the $_{nano}Pt_{(111)-(110)}$ sample, that contained the highest surface concentration of Pt(111) and Pt(110) sites. The CV experiment shown as solid lines (ten cycles) in Figure 8a (inset) was performed in clean supporting electrolyte after (i) removing the quinone-coated $_{nano}Pt_{(111)-(110)}$ electrode from 2 mM $H_2Q_{(aq)}$ and (ii) rinsing the electrode with clean supporting electrolyte solution to prevent transfer of $H_2Q_{(aq)}$ to the test cell. The arrows highlight the observed trend, i.e., a decrease in the process at ca. 0.06 V and a concomitant reappearance of features in the range of potentials associated to hydrogen UPD and (bi)sulfate adsorption at Pt(111) domains. The results suggest that the removal of the hydroquinone-derived adlayer, evident from the decreasing currents, takes place during the excursions to negative potentials in the hydroquinone-free supporting electrolyte. The presence of an isopotential point is consistent with the concomitant availability of decapped Pt(111) domains, formed as a direct product of the reductive desorption process. In fact, the reactivity of the $_{nano}Pt_{(111)(110)}$ sample is similar to the behavior exhibited by single crystal electrodes of the Pt(S)[(n − 1)(111)×(110)] stepped surface series (Figure S2) and is reminiscent of the behavior previously reported for $Q_{(ads)}$ layers at well-ordered Pt(111) single crystal electrodes in hydroquinone-free 0.5 M H_2SO_4.[26,28] In contrast, it sharply differs from the behavior at disordered Pt(111) single crystal electrodes[26,28] or at the lower basal planes,[26,28] i.e., Pt(110) and Pt(100). These experimental observations are consistent with expectations for a selective surface desorption process which requires the presence of well-ordered Pt(111) domains.

For reference, the tenth voltammogram (thick solid line) is compared with the CV for the clean surface (dashed line) in the mainframe (Figure 8b) using an expanded scale. At first glance, the steady voltammogram obtained after ten cycles does not reveal significant contributions because of processes associated to hydrogen or (bi)sulfate adsorption/desorption at the Pt(110) sites. The observation suggests that the removal of the hydroquinone-derived adlayer, during the excursions to negative potentials in the hydroquinone-free supporting electrolyte, takes place preferentially from well-ordered Pt(111) domains but not from Pt(110) sites. Recent in situ spectroelectrochemical experiments based on SNIFTIRS suggests that desorption of the full adlayer takes place at the negative potentials and that the molecules adsorb vertically onto the Pt(111) surface.[28] The desorption process in Figure 8a seems gradual because the reaction product, $H_2Q_{(aq)}$, can be readsorbed oxidatively

during the positive going scan under the conditions of the experiment.[28,29]

The recovery of other remaining Q-coated sites was attempted, after the tenth steady voltammogram, by subjecting the partly coated nanoparticles to a CO adsorption/oxidation cycle. The final CV experiment in Figure 8a (dashed line) was collected after bubbling high-purity $CO_{(g)}$ for 5 min while keeping the partly coated $_{nano}Pt_{(111)-(110)}$ electrode immersed in supporting electrolyte at 0.05 V. Under this condition, the displacement of any remaining $Q_{(ads)}$ by CO is expected. The resulting CV exhibits the small capacitive currents expected for the $_{nano}Pt_{(111)-(110)}$ electrode fully blocked by adsorbed CO, which has displaced $Q_{(ads)}$ from the $_{nano}Pt_{(111)-(110)}$ electrode surface and fully prevents hydrogen and (bi)sulfate adsorption.[26]

The third voltammogram in the main (expanded) frame of Figure 8b (thin solid line) was collected after electrochemical stripping of the $CO_{(ads)}$ layer. As can be observed, the final CV (thin solid line) closely traces the CV for the initially clean surface (dashed line). The result demonstrates that, within the conditions of the experiments, the adsorption/desorption of hydroquinone-derived adlayers does not disrupt the overall surface order or structure originally present at the $_{nano}Pt_{(111)-(110)}$ sample. It can safely be assumed, then, that the disappearance of the hydrogen and anion adsorption processes at the Pt(110) sites (thick solid line in Figure 8b) from previous experiments was related to the resilient adsorption of molecules at the Pt(110) sites and not to the disappearance of the surface sites via disordering or other phenomena.

This surface recovery strategy, was reproduced for the other two remaining $_{nano}Pt$ samples. These have a higher percent of Pt(100) surface sites and, for that reason, are better suited to evaluate reactivity at the Pt(100) sites. The results are shown in Figure S3 for $_{nano}Pt_{(111)-(100)}$ and in Figure 9 for a $_{nano}Pt_{(100)}$ electrode. As before, the sequence was (i) domain-selective reductive desorption of $Q_{(ads)}$ layers from ordered Pt(111) domains in clean supporting electrolyte (shown as consecutive solid-line voltammograms in the insets) to produce partly coated $_{nano}Pt$ samples (see the final steady CV in the inset which is expanded and reproduced as a thick solid line in the mainframe), (ii) full displacement of remaining $Q_{(ads)}$ layers using CO as a displacing ligand to form a compact layer of $CO_{(ads)}$ (see the dashed line CV in the insets corresponding to CO-blocked surface), followed by (iii) analysis of the recovered electrode surface (CV shown as thin solid line in the main frames) obtained after oxidation of the CO adlayers.

The $_{nano}Pt_{(100)}$ has the highest percentage of Pt(100) sites. Figure 9a (inset) was obtained in clean supporting electrolyte after (i) removing the quinone-coated $_{nano}Pt_{(100)}$ electrode from 2 mM $H_2Q_{(aq)}$ and (ii) rinsing the electrode with clean supporting electrolyte. A marked decrease in the process at ca. 0.06 V becomes apparent after repeated cycling. A concomitant reappearance of processes at Pt(111) domains is evident, especially in the range of potentials associated to hydrogen UPD and also in the (bi)sulfate adsorption region. The most prominent feature in the steady CV obtained after 10 cycles is the peak emerging at 0.26 V. This feature has been associated with hydrogen and (bi)sulfate adsorption at (100) edge terrace sites on the Pt(100) single crystal surfaces.[28] It is important to notice, however, that the feature for hydrogen and (bi)sulfate adsorption at well-orded Pt(100) terraces, ca. 0.37 V, is not recovered. The peak emerging at 0.26 V can be ascribed to the UPD of hydrogen and anion adsorption at "non-terrace" Pt(100) surface sites, likely at the edges of the nanoparticles. These sites become partly available upon cycling in 0.5 M H_2SO_4 solutions due to desorption of the organic adlayer, e.g., via re-equilibration of the surface coverage in the hydroquinone-free electrolyte solutions which may be assisted by the reductive desorption taking place at Pt(111) domains. Similar behavior has been reported at Pt(100) single crystal electrodes.[28] At Pt(100) single crystal surfaces, $Q_{(ads)}$ layers were reported to be remarkably stable at well-ordered Pt(100) domains but not at edges or imperfections. Both the scale and the mechanism for desorption at well-ordered Pt(100) was markedly different from that observed at the Pt(111) single crystal surfaces. The similarities between the previous results at Pt(100) single crystal surfaces and these new results at the preferentially oriented nanoparticles in the $_{nano}Pt_{(100)}$ electrode implies the presence of both well-ordered Pt(100) terraces and edges or defects with (100) character in the $_{nano}Pt_{(100)}$ sample.

The third voltammogram in the main (expanded) frame of Figure 9b (thin solid line) was collected after using CO as a displacing ligand. In this sample, the CV collected after CO adsorption/oxidation (thin solid line) closely traces the CV for the clean surface (dashed line). It is important to notice that after this treatment the hydrogen and anion adsorption processes at the Pt(110) sites and at the Pt(100) terraces are in fact mostly recovered. The results confirm that the adsorption/desorption of hydroquinone-derived adlayers does not disrupt the overall surface order or structure originally present at the $_{nano}Pt$ sample and that the disappearance of the hydrogen and anion adsorption processes at the Pt(110) sites and at Pt(100) terraces (thick solid line in Figure 9b) was in fact due to resilient adsorption of molecules at those surface sites and not to the disappearance of the surface sites via disordering, sintering, or other phenomena.

It will be noted, on closing, that some noteworthy differences do exist between the behavior of the redox process ascribed to eq 1 at Pt(*hkl*) single crystal surfaces and at nanoparticle surfaces. The FWHM was 22 mV at the Pt(111) surface which contrasts with the minimum value of 35 mV recorded at the $_{nano}Pt$ samples. The percent recovery of Pt(111) domains from Pt nanoparticles was better than that observed at the stepped single-crystal surfaces (not shown), which was likely due to the presence of adsorbed molecules at the Pt(110) step sites. Future efforts will be aimed at unraveling the possible role of adsorbate−adsorbate interactions at model Pt(*hkl*) and $_{nano}Pt$ surfaces in contact with systematically substituted aromatic molecules.

4. Conclusions

From the above discussion it may be concluded that the redox surface process ascribed to eq 1, i.e., reductive-desorption oxidative-chemisorption of hydroquinone-derived adlayers at Pt(111), is a highly selective surface process. In the forward direction, it requires the presence of well-ordered Pt(111) domains and is precluded at well-ordered Pt(100) terraces, at ordered Pt(110) terraces and steps, and at disordered Pt(111) electrode surfaces immersed in 2 mM $H_2Q_{(aq)}$. A good qualitative correlation is noted between the electrochemical behavior at well-ordered Pt(*hkl*) surfaces and at preferentially oriented Pt nanoparticles and, in this regard, this manuscript provides a proof-of-concept demonstration that preferentially oriented nanoparticles may serve as suitable model surfaces to study and to control aromatic molecular adsorption at the nanometer scale. From an analytical standpoint, it is demonstrated that in hydroquinone-containing solutions, the redox surface process may serve as a semiquantitative surface sensitive probe for

establishing the existence of well-ordered Pt(111) domains at metal−solution interfaces of any dimensionality. For the quinone−hydroquinone system, a quantitative charge balance between the measurements at single crystal electrodes and at nanostructured electrodes is not possible at this stage, i.e., higher than predicted charge densities are noted at the nanostructured electrodes. Possible sources of the bias include interferences emerging from side-reactions, e.g. HER, HOR, hydrogenation of molecules, etc., or from the underlying assumptions employed to attempt the quantitation, e.g., surface area measurements, scaling, double layer capacitance, limited type of surface sites at the model surfaces, etc.

Perhaps more noteworthy, the results suggest the technical feasibility of performing domain-selective decapping of nanoparticles controlled by the handle of an externally controlled parameter, i.e., in this case the electrode potential. This capability could be adapted to accomplish domain-selective adsorption of chemisorbates, such as metal adatoms or surface ligands (L) at Pt(111) domains of any dimension, including nanoparticle surfaces. Forward looking applications of domain selective reactivity could be visualized more readily by rewriting eq 1 in a more general form:

$$\frac{Q_{(ads)}}{Pt(111)} + 2e^- + 2H^+ + mL_{(aq)} \leftrightarrow m\frac{L_{(ads)}}{Pt(111)} + H_2Q_{(aq)} \quad (3)$$

Here, the domain-selective electrochemical reactivity is depicted as a ligand displacement reaction, where L represents any suitable ligand and m represents the numbers of ligands needed to displace a quinone molecule. Such atomic level control of composition at preferential surface domains in metal nanoparticle surfaces could aid in the design and engineering of new properties at electrocatalysts, electric contacts, and photonic devices. Future efforts will be aimed at testing such strategies for molecularly directed domain-selective surface deposition of adsorbates, metals, and ligands of interest at Pt group surfaces.

Acknowledgment. A.C.J. and M.R.L. appreciate the support from (i) the Pontifical Catholic University of Puerto Rico, (ii) the University of Puerto Rico-Mayaguez, and (iii) the Institute of Electrochemistry at University of Alicante through project CTQ 2006-04071/BQU.

Supporting Information Available: Additional information as noted in the text. This material is available free of charge via the Internet at http://pubs.acs.org.

JA909082S